RSC Advances

PAPER

View Article Online
View Journal | View Issue

Cite this: *RSC Adv.*, 2026, **16**, 22282

Protein hydrolysate derived from *Stichopus horrens* with antibacterial activity: preparation, characterization, and antibacterial mechanism

Hongrui Dong,[a] Jinhong Huang,[a] Lefan Li,[a] Pengzhi Hong[b] and Zhang Hu *[a]

Antimicrobial peptides from marine organisms are potential alternatives to small-molecule antibiotics. Sea cucumber protein hydrolysate (SPH) from *Stichopus horrens* was prepared through a physico-biological method, achieving a protein peptide content of 82.9%. Structural characterization by Ultraviolet, Fourier-transform infrared, and circular dichroism spectroscopies, and X-ray diffraction, revealed diverse bioactive peptides with α-helix (8.8%), β-sheet (32.1%), β-turn (23.9%), and random coil (35.1%) conformations. Inhibition zone assays demonstrated significant antibacterial activity against both Gram-positive and Gram-negative bacteria. Scanning electron microscopy indicated an antibacterial mechanism of SPH that involves disrupting bacterial cell membrane integrity, leading to content leakage and cell lysis. Three novel antimicrobial peptide sequences (QFLRVSGPLLKYPVVGPQ, ALGLPKCGPPLGPQ, and ALGLKCPPGPLGPQ) were identified by LC-MS/MS, and molecular docking suggested the potential interactions between antimicrobial peptides with the outer membrane protein BamA and the cytosolic protein Asd, providing supportive insights into possible membrane-associated and intracellular antibacterial mechanisms. This study provides a basis for developing novel sea cucumber-derived antimicrobial peptides with food and pharmaceutical applications.

Received 15th April 2026
Accepted 22nd April 2026

DOI: 10.1039/d6ra03185d

rsc.li/rsc-advances

1 Introduction

Antibiotics have been the primary means of preventing and treating bacterial diseases for a long time. However, with the overuse of antibiotics, the number of drug-resistant strains has surged, leading to a severe global public health crisis, making the development of novel antibacterial agents an urgent priority.[1] Antimicrobial peptides (AMPs), are natural substances present in diverse organisms that exhibit broad-spectrum antibacterial activity, low propensity for resistance development, and structural diversity, making them a key focus in the development of new antibacterial agents.[2] Natural products derived from plants, animals, and microorganisms represent an important source for AMPs discovery.[3] Numerous studies have confirmed the feasibility and effectiveness of isolating antimicrobial peptides from various natural sources.[4] Park *et al.*[5] successfully isolated a novel antimicrobial peptide, DLP, from hemolymphs of black soldier fly larvae through acid extraction and gel chromatography, and DLP exerts antibacterial activity against *Staphylococcus aureus* (*S. aureus*) by disrupting bacterial cell membrane integrity. Broekman *et al.*[6] isolated the antimicrobial peptide codCath from Atlantic cod *via* enzymatic hydrolysis, which rapidly killed bacteria through cell lysis and displayed activity against fungi and Gram-negative bacteria. Niknam *et al.*[7] isolated lactic acid bacteria from yogurt and purified the antimicrobial peptide BAPs using gel chromatography, and BAPs inhibited bacterial DNA polymerase activity and was effective against *Pseudomonas aeruginosa*, *Salmonella*, *Bacillus cereus*, and *S. aureus*. Ali *et al.*[8] extracted and purified antimicrobial peptide TroLEAP2 like-27 from mucus of golden pompano (*Trachinotus ovatus*) using high-performance liquid chromatography, and TroLEAP2 like-27 induced bacterial agglutination and acted on bacterial cell membranes, demonstrating antibacterial activity against *Lactococcus*, *S. aureus*, *Vibrio alginolyticus*, and *Vibrio harveyi*.

Sea cucumbers, belonging to phylum *Echinodermata* and class *Holothuroidea*, are marine invertebrates that inhabit a complex and variable seabed environment. To survive in such environments, sea cucumbers rely primarily on innate immune defenses against microbial invasion, these defenses include a variety of antibacterial substances.[9] Research and development of bioactive peptides from sea cucumbers has advanced, and these organisms are a key focus in marine bioprospecting. Using alkaline protease, Jayathilake *et al.*[10] isolated anti-aging protein peptides from the body wall of *Holothuria atra*, which effectively stimulated collagen activity in human dermal fibroblasts. Xu *et al.*[11] prepared sea cucumber collagen peptides (RDDPEPSYK) *via* pepsin and trypsin hydrolysis with potential anti-obesity applications as targeted pancreatic lipase

[a]*Faculty of Chemistry and Environmental Science, Guangdong Ocean University, Zhanjiang 524088, China. E-mail: huzhangqyx@126.com*
[b]*College of Food Science and Technology, Guangdong Ocean University, Zhanjiang 524088, China*

inhibitors. Zhao *et al.*[9] isolated and purified the antimicrobial peptide SCAK33 from sea cucumber proteomes, which exhibited strong antibacterial activity against *Bacillus megaterium*, *Bacillus subtilis*, and *Vibrio parahaemolyticus*. Huang *et al.*[12] prepared sea cucumber peptides with antioxidant effects, and in tumor-bearing mice the survival rate of the peptide-treated group was 2–3 times higher than that of the control group. Recent studies indicated that sea cucumber oligopeptides modulate protein processing pathways, promoting cell proliferation and wound healing.[13]

Developing antimicrobial peptides from natural marine products such as sea cucumbers represents a promising strategy to address antibiotic resistance and expand anti-infective therapeutic options.[14] In this study, sea cucumber protein hydrolysate (SPH) was prepared from *Stichopus horrens* (*S. horrens*) using a combined physico-biological approach. SPH was structurally and functionally characterized as illustrated in Fig. 1. We analyzed the peptide content, molecular weight distribution, and amino acid composition of SPH, and performed structural characterization using UV, FTIR, CD spectroscopy, and XRD. Antibacterial activity against common pathogens was confirmed by inhibition zone assays. Scanning electron microscopy revealed that SPH disrupts bacterial cell membranes. Additionally, LC-MS/MS combined with databases analysis predict three putative antimicrobial peptide sequences (QFLRVSGPLLKYPVVGPQ, ALGLPKCGPPLGPQ, ALGLKCPPGPLGPQ). Molecular docking further suggested potential interactions between these peptides and the outer membrane protein BamA as well as the cytosolic protein Asd, providing preliminary insights into their possible antibacterial mechanisms and identifying candidate peptides for further investigation.

2 Materials and methods

2.1 Materials

Fresh sea cucumber (*Stichopus horrens*) was purchased from a local seafood market in Zhanjiang, Guangdong, China. After removing sand and internal organs, samples were washed, cut into small pieces, frozen in liquid nitrogen, rapidly pulverized, and stored at −20 °C for use. The bacterial strains *Escherichia coli* (*E. coli*, ATCC 25922) and *Staphylococcus aureus* (*S. aureus*, ATCC 6538) were obtained from the Guangdong Microbial Culture Collection Center (GDMCC). Pepsin (30 U mg^{-1}), papain (800 U mg^{-1}), alkaline proteinase (200 U mg^{-1}) and bovine serum albumin (BSA) protein concentration assay kit

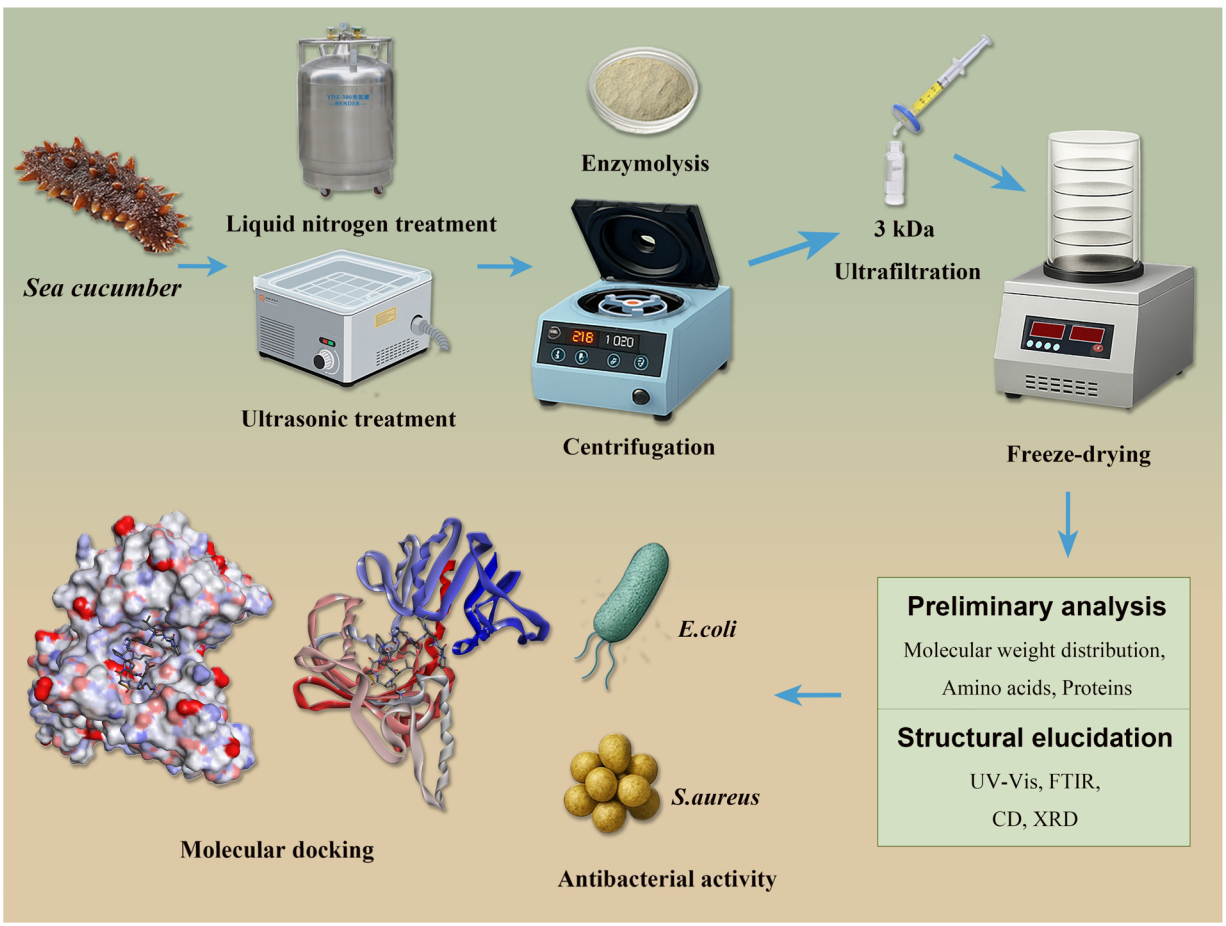

Fig. 1 The schematic diagram of sea cucumber protein hydrolysate (SPH) prepared from *S. horrens* using a combined physico-biological method, and systematically characterized its structural and antibacterial properties.

were purchased from Yuanye Bio-Technology Co. Ltd (Shanghai, China). All chemicals were of analytical grade and obtained from Sinopharm Chemical Reagent Co., Ltd (Shanghai, China).

2.2 Preparation of SPH

The pre-treated sea cucumber powder was suspended in distilled water and subjected to ultrasonication (300 W, 10 min). To enhance protein unfolding and improve hydrolysis efficiency, a stepwise pH-gradient sequential enzymatic hydrolysis strategy has been used. The pH was adjusted to the optimal value for enzymatic hydrolysis using 1 mol L^{-1} NaOH or HCl. Sequential digestion was performed using different enzymes (pepsin, papain, and alcalase, 3.0 kU mL^{-1}) at 50 °C for 6 h for each enzyme (pepsin pH 2.0, papain pH 7.0, and alcalase pH 8.5). The mixture was incubated in a boiling water bath for 10 min to inactivate the enzymes, followed by centrifugation (12 000 rpm, 20 min) to collect the supernatant. Anhydrous ethanol (3 : 1, v/v) was added and the solution was stored at 4 °C for 12 h. After centrifugation (12 000 rpm, 20 min), the supernatant was collected, concentrated, ultrafiltered through a 3 kDa cut-off membrane, and freeze-dried to obtain SPH.

2.3 Determination of peptide and amino acid content in SPH

Bicinchoninic acid (BCA) assay has been performed to determine the protein peptide content of SPH. Briefly, a BCA assay kit (Thermo Scientific, Waltham, USA) was used and six replicate wells for standard samples (each loaded with 20 μL of gradient-concentration bovine serum albumin standard protein solution) and one replicate well for the test sample (loaded with 20 μL of SPH solution) were prepared on a microplate. Subsequently, 200 μL of BCA working reagent was added to each well followed by thorough mixing. The plate was incubated at 37 °C for 30 min. After cooling to room temperature, the absorbance at 562 nm was measured using a microplate reader. A standard curve was generated in Origin software by plotting bovine serum albumin concentrations (μg mL^{-1}) on the *x*-axis against the mean A562 values of standards on the *y*-axis. The protein peptide concentration of SPH was calculated from the sample's A562 value using this calibration curve. In addition, amino acid composition and content were analyzed using an automatic amino acid analyzer (LA8080, HITACHI Co., Tokyo, Japan).

2.4 Molecular weight distribution of SPH

LC-MS/MS was performed using an EASY-nLC 1000 (Thermo Scientific, Waltham, USA) with a Pepmap RSLC C18 capillary column (75 μm × 150 mm, 2 μm, 00 Å) coupled to a Q-Exactive HF instrument (Thermo Scientific, Waltham, USA).[15] Samples were dissolved in 20 μL of 0.1% formic acid solution, vortexed thoroughly, and centrifuged (17000 g, 20 min) at 4 °C. The supernatant was determined, and the original data were processed using MaxQuant software.[16]

2.5 Structural characterization of SPH

2.5.1 UV. Samples were dissolved in distilled water to prepare a 0.05 mg mL^{-1} SPH solution, with distilled water as a blank control. Absorption spectra were recorded from 190 to 400 nm using a UV spectrophotometer (Mapada, Shanghai, China).

2.5.2 FTIR. Infrared spectra were obtained using the potassium bromide pellet method and an FTIR spectroscopy instrument (Alpha II, Bruker, Germany). Scanning parameters were wavenumber range 4000–500 cm^{-1}, 32 scans, and resolution 4 cm^{-1}. The secondary structure composition was quantified by deconvoluting the amide I band (1600–1700 cm^{-1}) in Origin using Gaussian–Lorentzian curve-fitting, with peak assignments based on characteristic wavenumbers.

2.5.3 CD. CD spectra were recorded from 190 to 260 nm with a scan rate of 50 nm min^{-1} and a sampling interval of 0.1 nm (JASCO-J1500, Shimadzu, Japan). Molar ellipticity $[\theta]$ was calculated using the following equation:[17]

$$[\theta] = \text{mdeg}/10LCN \quad (1)$$

where mdeg is the CD signal obtained from the instrument, L is the path length (cm), C is the concentration (mol L^{-1}) of samples, and N is the number of peptide residues.

2.5.4 XRD. XRD (Rigaku Ultima IV, Japan) analysis was performed using Cu Kα radiation at a scan rate of 5° min^{-1} over a 2θ range of 5–90°.

2.6 Zone of inhibition assay

E. coli and *S. aureus* were used as test strains. Bacterial suspensions in the logarithmic phase were diluted to 10^6 colony-forming units (CFU) mL^{-1} with sterile phosphate-buffered saline (PBS) and 100 μL was spread evenly on LB solid medium. Sterile Oxford cups were placed on the medium surface and 100 μL of sample solution with varied concentrations was added to each cup (dissolve 20 mg of the sample in distilled water to a volume of 50 mL, and then use the two-fold dilution method to obtain the test concentration solution). Gentamicin, a broad-spectrum antibiotic known to effectively inhibit both *E. coli* and *S. aureus*, was used as the positive control at a concentration of 50 μg mL^{-1}, and distilled water served as the negative control.[18–20] Petri dishes were incubated at 37 °C for 24 h and inhibition zones were photographed and measured using ImageJ.[21]

2.7 Bacterial cell morphology observation

To further decipher the antibacterial mechanism of SPH, the reference method[22] was employed to analyze the effects of SPH on bacterial cell membranes. Bacterial cells were treated with 2 mg mL^{-1} SPH solution for 6 h, with untreated bacteria serving as controls. Cells were washed three times with sterile PBS, centrifuged (4500 rpm, 10 min) at 4 °C, and resuspended in 2.5% glutaraldehyde for observation by SEM.

2.8 Antimicrobial peptide prediction

LC-MS/MS data were matched against known protein databases to obtain SPH peptide sequences in FASTA format. Sequences were analyzed using APD3 (https://aps.unmc.edu/prediction) and CAMPR3 databases (https://www.camp3.bicnirrh.res.in/index.php), and the sAMPpred-GAT tool (https://bliulab.net/sAMPpred-GAT/server), for antimicrobial peptide prediction.

2.9 Molecular docking analysis

Molecular docking was performed following as described by Wang *et al.*.[23] Receptor proteins BamA (PDB ID; 7nre, derived from *Escherichia coli* O157:H7) and Asd (PDB ID: 2yv3; derived from Thermus thermophilus HB8) were obtained from the PDB database. PyMOL was used to prepare the receptor structures by removing excess water molecules and small-molecule ligands, retaining only chain A.[24]

2.10 Statistical analysis

Unless otherwise stated, all results are presented as mean ± standard deviation (SD) of three independent replicates. Statistical analysis was performed using SPSS 26.0 and differences between groups were compared using independent-sample *t*-tests. A p-value < 0.05 (*) was considered statistically significant and $p < 0.01$ (**) was considered highly significant.

3 Results and discussion

3.1 Analysis of peptide and amino acid content in SPH

The protein peptide content of the prepared SPH was quantified using BCA assay. The standard curve fitting equation was $y = 1917.7x - 185.28$ ($R^2 = 0.9994$), and the measured protein peptide content in SPH was 82.9%. Amino acid composition analysis (Table 1) revealed the presence of 16 common amino acids in SPH, with a total content of 97.64 g/100 g. Among them, essential amino acids (EAAs) and non-essential amino acids (NEAAs) accounted for 26.19% and 71.45%, respectively, with an EAA/NEAA ratio of 0.37, similar to that reported for Parastichopus tremulus protein hydrolysate.[25] Notably, the hydrophobic amino acid content in SPH reached 35%. Studies have shown that when the hydrophobic amino acid content in a protein/peptide system exceeds 31.5%, a semi-transparent gel can form. Among the amino acids, glutamic acid was the most abundant (17.1%), which promotes the activation and proliferation of natural killer cells and T cells, enhancing cellular immunity.[26] Glycine (14.7%), an important component of collagen, plays a vital role in maintaining the health of tissues such as skin and joints.[27] Additionally, SPH contained abundant antibacterial amino acids including proline (9.73%) and arginine (8.06%). Studies indicate that proline exerts antibacterial effects by binding to bacterial cell membranes and forming transient pores for intracellular transport.[28] Arginine exhibits antibacterial activity through other mechanisms.[29] Further analysis showed that among every 1000 amino acid residues, glycine was the most frequent (226 residues), accounting for approximately one-fifth of total amino acids, consistent with the findings of Feng *et al.*[30] Meanwhile, the total number of cationic amino acids (arginine, lysine, and histidine) with antibacterial properties was 124, similar to previously reported results.[31,32] Moreover, the total free amino acid content was 0.98 g/100 g, which can act as an osmotic regulator in cell volume adjustment.[33] Studies by Langevin *et al.*[34] and Pismenskaya *et al.*[35] demonstrated that H^+ and OH^- ions generated by water dissociation can react with free amino acids and peptides, thereby

Table 1 Amino acid composition and content of SPH (dry basis)

	Content (g/100 g)	Amino acid residues/1000 total amino acid residues	Content (g/100 g)
Amino acids	Total amount of amino acids	Total amount of amino acids	Free amino acids
Asp	8.85	78	0.02
Thr[b]	2.99	30	0.02
Ser	4.18	48	0.03
Glu	17.1[c]	147	0.02
Gly	14.7[c]	226	0.18
Ala	6.95	89	0.06
Val[b]	3.32	38	0.07
Met[b]	0.93	9	0.03
Ile[b]	2.63	27	0.13
Leu[b]	5.34	46	0.12
Tyr	1.88	18	0.01
Phe[b]	3.64	25	0.04
Lys[a,b]	5.70	47	0.02
His[a,b]	1.64	19	0.08
Arg[a]	8.06	58	0.12
Pro[a]	9.73	95	0.03
Total	97.64	1000	0.98

[a] Antibacterial amino acids. [b] Essential amino acids. [c] The abundant amino acids are in bold.

promoting interactions between bioactive peptides and cell membranes.

3.2 LC-MS/MS analysis

Molecular weight (MW) distribution analysis of SPH (Table 2) showed that the majority of SPH components (96.55%) had a MW below 3000 Da, with 77.79% of components below 1000 Da. This indicates that SPH primarily consists of low MW bioactive peptides. The predominance of low MW components theoretically endow SPH with favorable water solubility and absorption properties. Structural quality criteria (*e.g.*, MW, amino acid composition, and peptide sequence) are key factors influencing peptide bioactivity.[36] Low MW peptides generally exhibit more pronounced bioactivity with good potential for pharmaceutical and functional food development.[37] Lu *et al.*[38] reported that sea cucumber peptides with MW < 3000 Da possess superior functional activity. Xu *et al.*[11] found that lower MW significantly enhances the metal ion-chelating capacity of sea cucumber peptides, thereby improving their antibacterial activity. Safari *et al.*[39] and Zou *et al.*[36] reported that lower MW significantly improves the antioxidant activity of peptides. Therefore, the prepared SPH, characterized by its low MWs, represents a peptide pool enriched with certain bioactive-related components, whose activity ultimately depends on specific amino acid sequences and spatial structures.

3.3 UV spectroscopy analysis

In the UV spectrum of SPH (Fig. 2a), a characteristic peptide bond absorption peak ($\pi \rightarrow \pi''$ transition) was observed at ~200 nm, directly reflecting the conjugated structure (–CO–NH–) of peptide bonds. This sharp and prominent peak indicated abundant peptide components in the sample. In the 250–280 nm wavelength range, weak characteristic absorption signals of aromatic amino acids were detected, consistent with the low content of aromatic amino acids (Tyr and Phe) (<5% in total) revealed by amino acid composition analysis. Notably, the baseline of the UV spectrum was stable without abnormal impurity peaks, suggesting no obvious UV-detectable impurities and a high sample purity (peptide content 82.9%). This spectral feature closely resembled the active peptide fractions from Stichopus monotuberculatus reported by Zhong *et al.*,[37] implying that protein hydrolysates from different sea cucumber species may share conserved structural characteristics.

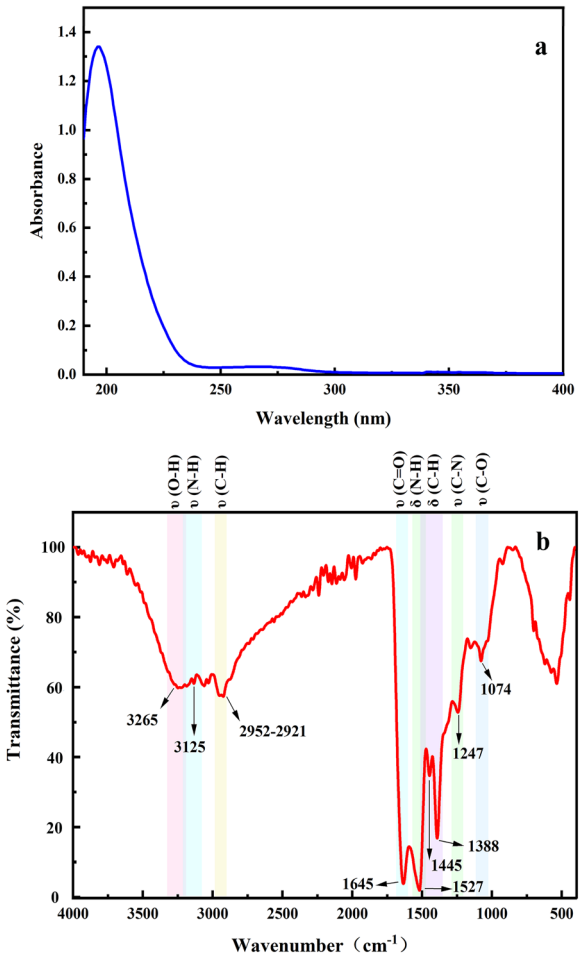

Fig. 2 UV (a) and FTIR (b) spectra of SPH.

3.4 FTIR spectroscopy

FTIR spectroscopy is an effective method for identifying vibrational modes of functional groups and intermolecular interactions. The FTIR spectrum of SPH (Fig. 2b) exhibited characteristic absorption peaks at 3265 cm^{-1} (amide A band), 3125 cm^{-1} (amide B band), 2952 cm^{-1} and 2921 cm^{-1} (C–H stretching vibrations), 1645 cm^{-1} (amide I band), 1527 cm^{-1} (amide II band), and 1247 cm^{-1} (amide III band). These peak positions were consistent with previously reported spectra of sea cucumber peptides/proteins, confirming the presence of

Table 2 Molecular weight distribution of SPH

Molecular weight range (D_a)	Peak area percentage (%)	Number-average molecular weight (M_n)	Weight-average molecular weight (M_w)
>5000	0.74	9633	4372
5000–3000	2.70	3777	3857
3000–2000	5.75	2416	2449
2000–1000	13.01	1368	1423
1000–500	19.62	672	697
500–189	35.88	281	306
<189	22.29	—	—

typical peptide/protein functional groups in SPH.[40–42] To further elucidate the secondary structure composition, deconvolution of the amide I band (1600–1700 cm^{-1}) was performed. The analysis revealed a secondary structure distribution of 8.7% α-helix, 33.2% β-sheet, 24.5% β-turn, and 33.6% random coil.[43] Notably, the amide A band (3265 cm^{-1}) and amide II band (1527 cm^{-1}) appeared at lower wavenumbers than their typical ranges (3500–3300 cm^{-1} and 1530–1550 cm^{-1}, respectively), indicating a red shift. The red shift of the amide A band suggests N–H group participation in hydrogen bond formation,[34] while that of the amide II band implies enhanced hydrogen bonding interactions.[41] Therefore, a strong hydrogen bond network is formed in SPH, which plays a crucial role in maintaining the stable spatial structures of its components,[34,38,41] and that may be associated with its bioactivities.

3.5 CD

CD spectroscopy rapidly analyzes the secondary structure composition (*e.g.*, α-helix, β-sheet, and random coil content) of chiral substances (*e.g.*, proteins/peptides) in solution by measuring their differential absorption of polarized light, making it widely applicable in protein/peptide structural analysis.[44] To elucidate the secondary structure composition of antimicrobial peptides in SPH, CD spectroscopy was performed (Fig. 3a). The CD spectrum displayed a negative absorption peak at 190–222 nm, characteristic of α-helical structures.[41–43] A positive CD signal was observed at ~218 nm, accompanied by a negative signal at shorter wavelengths, indicating the presence of β-sheet structures.[45] A negative CD signal at 200–205 nm was attributed to random coils. Quantitative analysis of the spectral data using CDPro software (Fig. 3b) revealed the secondary structure composition of SPH as 8.8% α-helix, 32.1% β-sheet, 23.9% β-turn, and 35.1% random coil, totaling 99.9% (the value of normalized root mean square deviation = 0.143).[46] This composition closely matches the active peptide results reported by Chen *et al.*[16] Furthermore, FTIR amide I analysis revealed consistent structural trends, which served to reinforce and validate the secondary structure results derived from CD spectroscopy.[47]

3.6 XRD

XRD is a valuable technique for analyzing the structure of crystalline compounds. The XRD pattern of SPH (Fig. 3c) showed a sharp diffraction peak at $2\theta = 20.28°$, assigned to the (100) crystal plane of the monoclinic system with an intensity of ~7000 a.u., confirming the presence of a highly ordered crystalline structure, consistent with the findings by Huang *et al.*[12] The sharp morphology of the (100) diffraction peak indicated small crystallite size, high crystallinity, and regular atomic periodicity along this direction.[48] Additionally, broad diffuse peaks (intensity 2000–4000 a.u.) were observed in the 30–45° range, suggesting the coexistence of amorphous regions. This dual crystalline-amorphous structure of SPH synergistically enhances its antibacterial function; crystalline regions provide rigidity to facilitate bacterial cell membrane penetration, while amorphous regions confer molecular flexibility to adapt to the binding sites of target proteins (*e.g.*, BamA, and Asd), thereby cooperatively achieving efficient membrane disruption.

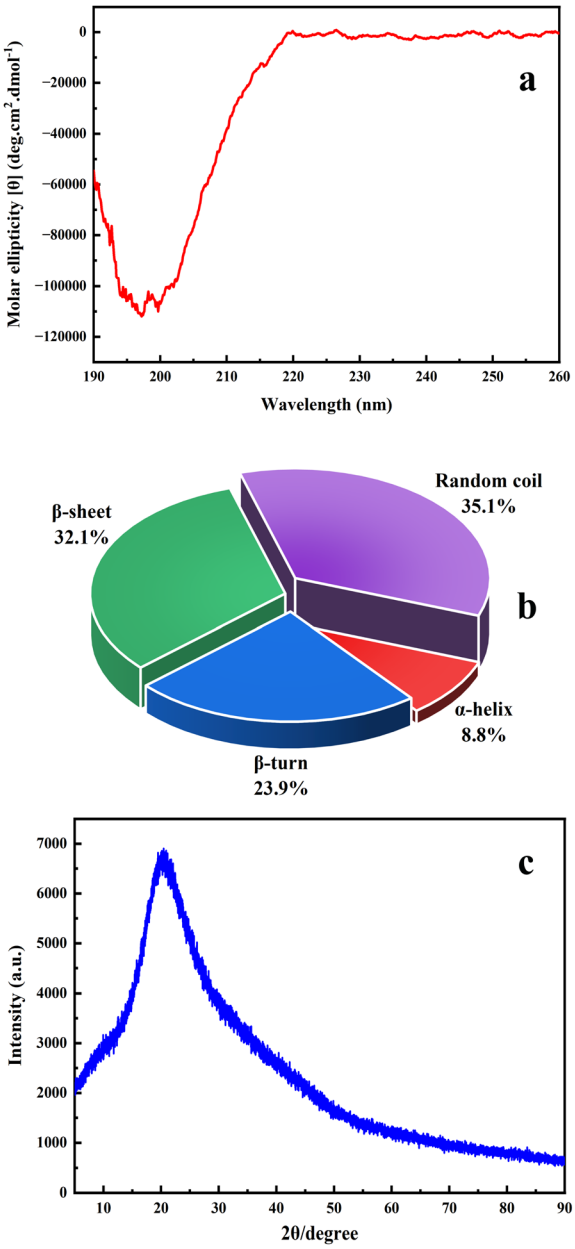

Fig. 3 (a) The CD spectra of SPH; (b) quantitative analysis results of secondary structure of SPH; (c) the XRD pattern of SPH.

3.7 Determination of antibacterial activity

The antibacterial activity of SPH was tested against *S. aureus* and *E. coli* using the inhibition zone method, with distilled water and gentamicin as the blank and positive controls, respectively (Fig. 4). The blank control group showed robust bacterial growth with no inhibition zones, and the positive control yielded inhibition zones of 13.7 ± 0.5 mm and 13.5 ± 0.3 mm against *S. aureus* and *E. coli*, respectively. As for the samples, SPH at all tested concentrations (1, 2, and 4 mg mL^{-1}) produced distinct inhibition zones, the diameters of which

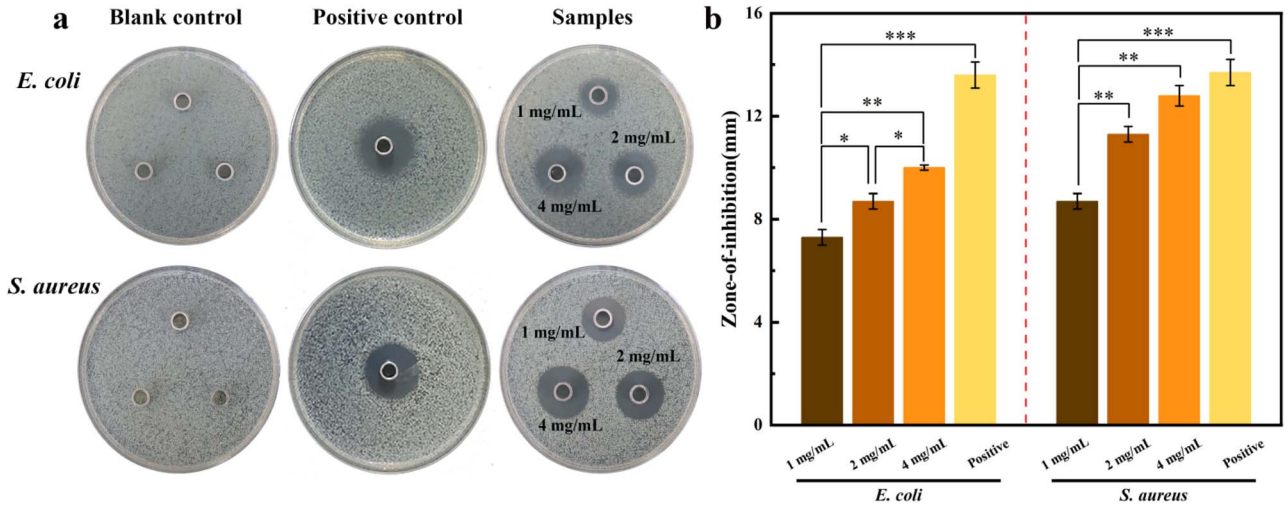

Fig. 4 (a) The digital image, and (b) the bar chart analysis of zone-of-inhibition.

increased with SPH concentration, indicating a concentration-dependent effect. The inhibition zone diameters of SPH (1, 2, and 4 mg mL^{-1}) against *S. aureus* were 8.7 ± 0.3, 11.3 ± 0.4, and 12.8 ± 0.4 mm, respectively, while those against *E. coli* were 7.3 ± 0.2, 8.7 ± 0.3, and 10.0 ± 0.2 mm, respectively. The comparisons between groups revealed significant differences ($p < 0.05$) among all concentrations for *E. coli*, whereas for *S. aureus* the differences between 1 mg mL^{-1} and higher concentrations (2 and 4 mg mL^{-1}) were highly significant ($p < 0.01$). In summary, SPH exhibited significant antibacterial activity against both test strains, with superior efficacy against *S. aureus* compared with *E. coli*,[49] attributable to their distinct outer membrane structures. Gram-positive bacteria possess a thick peptidoglycan layer (bearing negatively charged teichoic acids), whereas Gram-negative bacteria have a triple-layered barrier (hydrophobic outer membrane, peptidoglycan layer, and cell membrane), which hinders the penetration of antibacterial molecules, thereby reducing the effectiveness of SPH against *E. coli*.[50] Meanwhile, Piri-Gharaghie *et al.* found that the sea cucumber methanolic extracts had similar antibacterial properties against *Staphylococcus aureus*, *Streptococcus mutans*, *Porphyromonas gingivalis*, and *Tannerella forsythia*.[51]

3.8 Bacterial cell morphology analysis

To investigate the mechanism of the antibacterial action of SPH, bacterial cell morphology was examined using SEM (Fig. 5). Cells in the *E. coli* control group were intact short rods (length 1.5–2.0 μm, diameter 0.5 μm) with smooth, undamaged surfaces, while those in the *S. aureus* control group were uniformly-sized (diameter 0.8–1.0 μm) and spherical with continuous, unblemished surfaces. In contrast, SPH-treated *E. coli* cells displayed severe surface wrinkling, fractures, localized depressions, and mid-cell constriction (~30% length reduction), with flocculent content leakage at rupture sites. Similarly, SPH-treated *S. aureus* cells exhibited pronounced structural damage, including 50–100 nm pores, crescent-shaped deformities, and partial cell disintegration. These marked morphological alterations indicate that SPH compromised bacterial cell wall/membrane integrity, manifesting as pore formation, structural collapse, cellular content leakage, and ultimately, cytoskeletal disintegration and cell lysis. These findings align with reports by Imperlini *et al.*[52] and Zhao *et al.*,[9] indicating that amphipathic α-helical antimicrobial peptides bind bacterial cell membranes *via* cationic regions interacting with phospholipid bilayers, while hydrophobic segments insert into the lipid core.[49,50] Upon reaching a threshold concentration, these peptides alter membrane tension, forming transmembrane pores that induce cytoplasmic content efflux and bacterial death. These observations suggest that SPH may exert its antibacterial activity primarily through membrane-related mechanisms, while the involvement of specific molecular interactions requires further investigation at the protein level.

3.9 Screening and prediction of putative antimicrobial peptides

Through LC-MS/MS analysis, total ion chromatograms (TIC), base peak intensity chromatograms (BPC), and mass spectra of

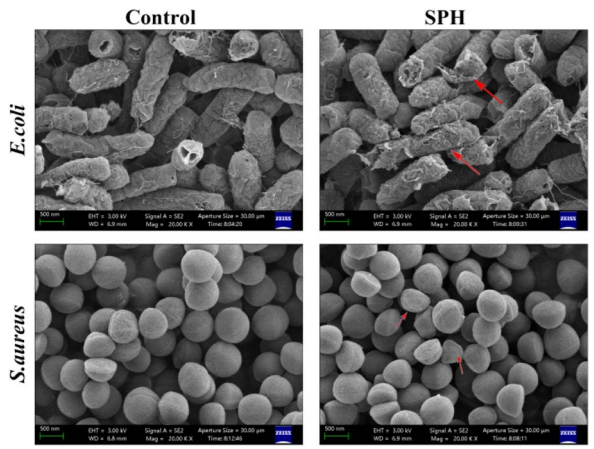

Fig. 5 The cell morphology of *E. coli* and *S. aureus* observed by SEM.

SPH samples were obtained (Fig. 6a–c). A database search of the acquired 6019 spectra successfully matched 281 spectra, identifying 130 peptides and 139 proteins (Fig. 6d).[53] Subsequently, three prediction tools—APD3 (comprehensive analysis based on spatial parameters of known antimicrobial peptides), CAMPR3 (utilizing SVM, RF, and ANN algorithms), and sAMPpred-GAT (based on graph attention networks)—were employed to predict the antibacterial activity of all identified peptides. Based on this screening strategy, three potential antimicrobial peptides, QFLRVSGPLLKYPVVGPQ (Named QQ-18-1), ALGLPKCGPPLGPQ (AQ-14-6), and ALGLKCPPGPLGPQ (AQ-14-7) (Table 3), were ultimately identified and subjected to molecular docking studies to explore their antibacterial mechanisms.

3.10 Molecular docking

Molecular docking is a computational simulation method used to explore interactions between molecules and predict their binding modes and affinities.[54] To investigate the mechanism of SPH in depth, molecular docking was performed to examine the potential interactions between SPH-derived peptides and the representative bacterial target proteins.[16] Peptide-ligand conformations were predicted using the ColabFold tool based on Alphafold,[55] and the models with the highest scores of pLDDT (Predicted Local Distance Difference Test) (QQ-18-1 pLDDT = 70.1, AQ-14-6 pLDDT = 77.4, and AQ-14-7 pLDDT = 75.9) were selected for molecular docking using AutoDock Vina 1.1.2.[56] The molecular docking results showed that antimicrobial peptides in SPH (QQ-18-1, AQ-14-6, and AQ-14-7) formed stable complexes with two representative bacterial proteins: *E. coli* protein BamA[57] and the enzyme Asd (Aspartate-semialdehyde dehydrogenase) from *S. aureus*.[23] Although Asd is a cytosolic protein, previous studies have shown that antimicrobial peptides can penetrate bacterial membranes and subsequently interact with intracellular targets, thereby exerting synergistic antibacterial effects. The binding energies of all optimal docking conformations [BamA/QQ-18-1 (-6.1 kcal mol^{-1}), BamA/AQ-14-6 (-6.2 kcal mol^{-1}), BamA/AQ-14-7 (-5.0 kcal mol^{-1}), Asd/QQ-18-1 (-6.4 kcal mol^{-1}), Asd/AQ-14-6 (-7.1 kcal mol^{-1}), and Asd/AQ-14-7 (-6.9 kcal mol^{-1})] were ≤ -5 kcal mol^{-1}, meeting the energy criteria for stable complexes,[56] confirming strong interactions between the ligands (SPH) and receptors (target proteins) and the structural stability of the complexes. Further analysis of specific binding modes revealed that QQ-18-1 precisely localizes to the membrane-side gate region of BamA (Fig. 7a–c), formed by β1-β16 strands, which constitutes the functional "Lateral Gate" essential for the folding and insertion of nascent outer membrane proteins OMPs into the lipid bilayer.[58,59] Gly 384 on the β16 strand adopts a critical random coil conformation within this gate,[23] the binding of QQ-18-1 to this conserved functional area likely restricts the conformational flexibility of the β-barrel, thereby obstructing the OMP biogenesis pathway.[60] Meanwhile, QQ-18-1 forms hydrogen bonds with Asd residues Glu 206, Arg 231, Asp 196, and Arg 37, while engaging in significant hydrophobic interactions with residues such as Gly7 and Gly158 (Fig. 7d–f). Structural mapping indicates that these residues are located within the catalytic active site and substrate-binding pocket of Asd. As Asd is a key enzyme in the diaminopimelic acid (DAP) biosynthetic pathway,[61,62] the occupancy of this active site by SPH peptides directly impairs the synthesis of essential cell wall precursors. This specific binding pattern provided important mechanistic insights: it validated the classical action pathway of antimicrobial peptides[23]—positively-charged SPH targets negatively charged bacterial cell membranes *via* electrostatic attraction, subsequently forming stable hydrogen bond and hydrophobic interaction networks with the aforementioned functional domains of key proteins (*e.g.*, BamA and Asd), directly disrupting their biological functions.[63] Notably, AQ-14-6 and AQ-14-7 exhibited highly similar interaction patterns with the key functional sites of target proteins (Fig. S1 and S2). In summary, molecular docking simulations showed that SPH likely exerts its potent antibacterial activity by specifically binding to and disrupting key functional areas of membrane integrity-maintaining proteins such as BamA and Asd, ultimately leading to bacterial cell membrane dysfunction and metabolic inhibition. This provides a structural basis for understanding its high antibacterial efficacy. When considered together with SEM observations and antibacterial assays, these results support a multi-level antibacterial

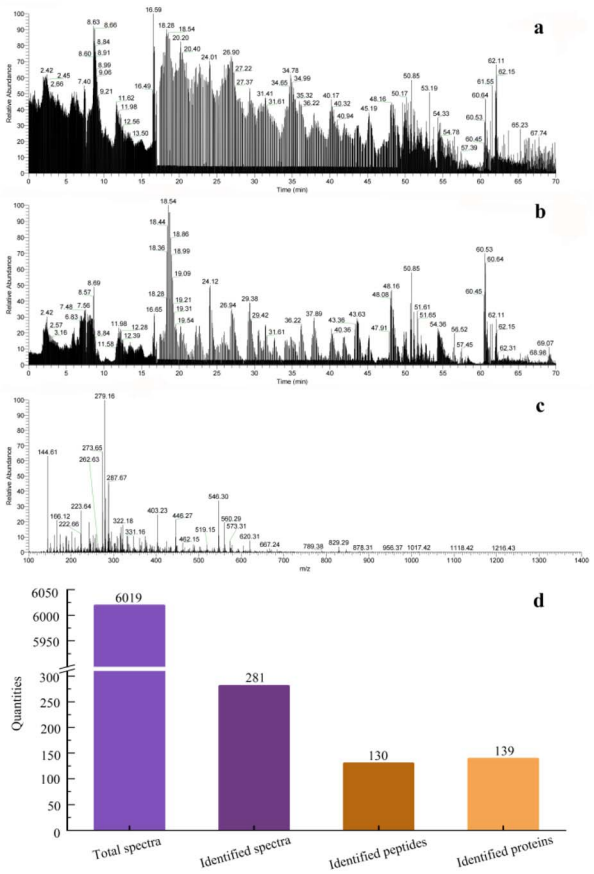

Fig. 6 (a) The TIC chromatogram; (b) BPC chromatogram; (c) mass spectra of SPH; and (d) the spectrum quantization identified by LC-MS/MS.

Table 3 Prediction of potential antimicrobial peptides[a]

Peptide name	Peptide sequence	APD3	CAMP			
			SVM	RF	ANN	sAMPpred-GAT
QQ-18-1	QFLRVSGPLLKYPVVGPQ	+	0.598	0.575	+	+
AQ-14-6	ALGLPKCGPPLGPQ	+	0.611	0.508	+	+
AQ-14-7	ALGLKCPPGPLGPQ	+	0.543	0.509	+	+

[a] Note: "+" and positive values indicate potential antimicrobial peptides.

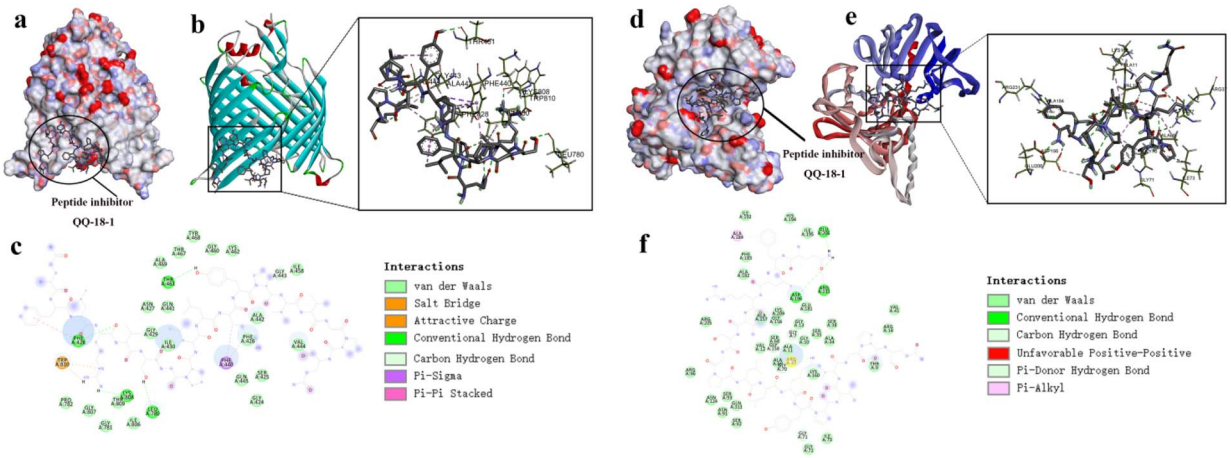

Fig. 7 Molecular docking diagram of antibacterial peptide QQ-18-1 binding to BamA and Asd proteins. (a) Top view of antibacterial peptide QQ-18-1 binding to BamA protein; (b) the binding mode of antibacterial peptide QQ-18-1 with BamA protein; (c) 2D interaction of antimicrobial peptide QQ-18-1 with BamA protein; (d) top view of antibacterial peptide QQ-18-1 binding to Asd protein; (e) The binding mode of antibacterial peptide QQ-18-1 with Asd protein; (f) 2D interaction of antimicrobial peptide QQ-18-1 with Asd protein.

mechanism, in which membrane disruption appears to be the primary mode of action, while predicted peptide-protein interactions may further enhance the overall antibacterial effect in a synergistic manner.

4 Conclusions

In this study, SPH was successfully prepared and its antibacterial properties were systematically investigated, providing new insights for the development of novel antibacterial agents. SPH was prepared through various physical treatments (liquid nitrogen flash-freezing, mechanical pulverization, ultrasonic cavitation) combined with composite enzymatic hydrolysis, which effectively preserved its bioactive components, yielding a high peptide content of 82.9%. Structural characterization of SPH using CD spectroscopy and other techniques revealed diverse active peptide structures, which may be closely related to its antibacterial activity (α-helix 8.8%, β-sheet 32.1%, β-turn 23.9%, and random coil 35.1%). The antibacterial activity of SPH was evaluated using the inhibition zone method, and SPH exhibited significant antibacterial effects. The investigations of antibacterial mechanisms based on SEM observations indicated that SPH primarily disrupted bacterial cell membrane integrity, leading to membrane disruption and cellular damage. Furthermore, LC-MS/MS was employed to identify and analyze the amino acid sequences of peptides in SPH, leading to the identification of three potentially bioactive peptides (QFLRVSGPLLKYPVVGPQ, ALGLPKCGPPLGPQ, and ALGLKCPPGPLGPQ) with antibacterial properties. Molecular docking simulations were performed between these peptides and two representative bacterial proteins, including the key protein BamA and Asd. The docking results suggested favorable binding interactions, providing theoretical and supportive insights into the potential antibacterial mechanisms of SPH. Nevertheless, it should be emphasized that these findings are preliminary. Although our enrichment steps yielded a peptide content of 82.9%, the remaining 17.1% of the sample consists of non-peptide compounds, such as residual carbohydrates, lipids, or other small molecules. Consequently, the observed antibacterial activity cannot be unequivocally attributed solely to the peptide fraction at this stage. Future studies using individual peptides are necessary to experimentally validate their antibacterial targets and mechanisms of action.

Author contributions

Hongrui Dong: conceptualization, methodology, investigation, formal analysis, writing – original draft preparation. Jinhong Huang: software, investigation, validation. Lefan Li: data curation, visualization, validation. Pengzhi Hong: resources,

supervision, writing – review & editing. Zhang Hu: conceptualization, project administration, funding acquisition, writing – review & editing.

Conflicts of interest

There are no conflicts to declare.

Data availability

The data included in this article are available on request.

Supplementary information (SI): two peptides, AQ-14-6 and AQ-14-7, interact with BamA and Asd through molecular docking analysis. See DOI: https://doi.org/10.1039/d6ra03185d.

Acknowledgements

This research was funded by Guangdong Provincial Natural Science Foundation of China (2024A1515012618 and 2026A1515010006) and Key Projects of Colleges and Universities in Guangdong Province (2022ZDZX2027).

References

1 K. A. Kanaujia, S. Wagh, G. Pandey, V. Phatale, P. Khairnar, T. Kolipaka, P. S. Rajinikanth, S. A. Saraf, S. Srivastava and S. Kumar, *Int. J. Biol. Macromol.*, 2025, **307**, 142158.
2 F. Tian, S. Rodtong, K. Thumanu, Y. Hua, S. Roytrakul and J. Yongsawatdigul, *Foods*, 2022, **11**, 3564.
3 M. Czelej, T. Czernecki, K. Garbacz, J. Wawrzykowski, M. Jamioł, K. Michalak, N. Walczak, A. Wilk and A. Waśko, *Foods*, 2023, **12**, 3394.
4 S. García-Vela, A. Cournoyer, Z. Sánchez-Reinoso and L. Bazinet, *Foods*, 2025, **14**, 8.
5 S.-I. Park, J.-W. Kim and S. M. Yoe, *Dev. Comp. Immunol.*, 2015, **52**, 98–106.
6 D. C. Broekman, A. Zenz, B. K. Gudmundsdottir, K. Lohner, V. H. Maier and G. H. Gudmundsson, *Peptides*, 2011, **32**, 2044–2051.
7 M. Niknam, L. Sadeghi and G. Zarrini, *Microb. Pathog.*, 2025, **204**, 107537.
8 W. Ali, Y. Chen, Z. Wang, M. Sun, Y. Song, X. Guo, X. Wang, Y. He and J. Qi, *Fish Shellfish Immunol.*, 2025, **162**, 110310.
9 Y. Zhao, L. Hao, Y. Meng, L. Li, W. Wang, R. Zhao, P. Zhao, J. Zhang, M. Wang, J. Ren, L. Zhang, X. Yin and X. Xia, *Int. Microbiol.*, 2025, **28**, 1019–1031.
10 N. J. Jayathilake, N. D. Wimalagunarathna, I. Wijesekara and V. K. Gunathilake, *Asian J. Biotechnol. Bioresour. Technol.*, 2023, **9**, 41–51.
11 Z. Xu, J. Chang, Z. Qin, H. Liu, X. Yan, S. Guan, X. Dong, J. Wu and T. Li, *Food Biosci.*, 2025, **65**, 106013.
12 S. Huang, K. Wang, Z. Hua, A. M. Abd El-Aty and M. Tan, *Int. J. Biol. Macromol.*, 2023, **253**, 127039.
13 B. Mazumder, M. Lu, H. Rahmoune, A. Fernandez-Villegas, E. Ward, M. Wang, J. Ren, Y. Yu, T. Zhang, M. Liang, W. Li, N. F. Läubli, C. F. Kaminski and G. S. Kaminski Schierle, *Biomed. Pharmacother.*, 2024, **180**, 117466.
14 M.-L. Heymich, S. Srirangan and M. Pischetsrieder, *Foods*, 2021, **10**, 1192.
15 J. Manguy, G. I. Papoutsidakis, B. Doyle and S. Trajkovic, *Foods*, 2025, **14**, 1180.
16 G. Chen, X. Ge, Y. Sun, W. Sui, Y. Jin, J. Geng, M. Zhang and T. Wu, *Int. J. Biol. Macromol.*, 2025, **295**, 139499.
17 A. Frontera and S. Emamian, *J. Phys. Chem. A*, 2025, **129**, 1368–1385.
18 P. Chevallier, H. J. Wiggers, F. Copes, C. Zorzi Bueno and D. Mantovani, *Nanomaterials*, 2023, **13**, 484.
19 W. Ratnasooriya, R. Wijerathna, N. Asanthi, N. R. M. Nelumdeniya and J. Pharmacogn, *Phytochem.*, 2018, **7**, 639–642.
20 P. Ngamsurach and P. Praipipat, *Heliyon*, 2022, **8**, e11704.
21 T. Thilagashanthi, K. Gunasekaran and K. S. Satyanarayanan, *J. Clean. Prod.*, 2021, **324**, 129217.
22 H. Dong, L. Liao, P. Yu, B. Long, Y. Che, L. Lu and B. Xu, *Bioorg. Chem.*, 2023, **140**, 106764.
23 M. Wang, H. Yue, Y. Bo, H. Yin, Y. Tian, Z. Zhao, C. Xue, T. Zhang and Y. Wang, *Food Biosci.*, 2024, **61**, 104390.
24 J. He, H. Li, Y. Xu, Y. Li, T. Yang, X. Yu, X. Yang, A. Huang, Y. Yu and Y. Shi, *J. Dairy Sci.*, 2025, **108**, 3428–3443.
25 J. Mildenberger, M. Remm and M. Atanassova, *LWT*, 2021, **148**, 111678.
26 D. L. Aminin, C. Koy, P. S. Dmitrenok, B. Müller-Hilke, D. Koczan, B. Arbogast, A. A. Silchenko, V. I. Kalinin, S. A. Avilov, V. A. Stonik, P. D. Collin, H.-J. Thiesen, M. L. Deinzer and M. O. Glocker, *J. Proteomics*, 2009, **72**, 886–906.
27 P.-H. Li, W.-C. Lu, Y.-J. Chan, W.-C. Ko, C.-C. Jung, D. T. Le Huynh and Y.-X. Ji, *Aquaculture*, 2020, **515**, 734590.
28 G. K R, R. Balenahalli Narasingappa and G. Vishnu Vyas, *Heliyon*, 2024, **10**, e38079.
29 T. Abraham, E. J. Prenner, R. N. A. H. Lewis, C. T. Mant, S. Keller, R. S. Hodges and R. N. McElhaney, *Biochim. Biophys. Acta, Biomembr.*, 2014, **1838**, 1420–1429.
30 J. Feng, H. Wang, X. Luo, L. Zhang and P. Zhou, *Int. J. Biol. Macromol.*, 2024, **279**, 134958.
31 X. Zhao, Y. Liu, Y. Li, X. Zhang and H. Qi, *Food Control*, 2018, **91**, 128–137.
32 Y. Liu, Q. Zheng, M. Tan, Z. Chen, H. Zheng, J. Gao, H. Lin, G. Zhu and W. Cao, *Int. J. Biol. Macromol.*, 2025, **294**, 139321.
33 D. Huo, L. Zhang, H. Yang and L. Sun, *Environ. Pollut.*, 2023, **330**, 121766.
34 M.-E. Langevin and L. Bazinet, *J. Membr. Sci.*, 2011, **369**, 359–366.
35 N. D. Pismenskaya, E. I. Belova, V. V. Nikonenko and C. Larchet, *Russ. J. Electrochem.*, 2008, **44**, 1285–1291.
36 T. B. Zou, T. P. He, H. B. Li, H. W. Tang and E. Q. Xia, *Molecules*, 2016, **21**, 72.
37 M. Zhong, T. Chen, C. Hu and C. Ren, *J. Food Sci.*, 2015, **80**, C671–C679.
38 Z. Lu, J. Yang, X. Xu, R. Liu and S. Lin, *Eur. J. Pharmacol.*, 2024, **968**, 176430.
39 R. Safari and Z. Yaghoubzadeh, *Int. J. Pept. Res. Ther.*, 2020, **26**, 2393–2398.

40 L. Xiao, J. Lv, Y. Liang, H. Zhang, J. Zheng, F. Lin and X. Wen, *LWT*, 2023, **173**, 114294.
41 S. Pezeshk, M. Rezaei and M. Abdollahi, *Ultrason. Sonochem.*, 2022, **89**, 106129.
42 H. Zheng, M. Zhao, Q. Dong, M. Fan, L. Wang and L. Li, *Food Hydrocoll.*, 2022, **132**, 107849.
43 L. Devkota, K. Kyriakopoulou, R. Bergia and S. Dhital, *Foods*, 2023, **12**, 908.
44 Y. Dong and Z. Dai, *Mar. Drugs*, 2022, **20**, 550.
45 S. Pakrashy, P. K. Mandal, S. Paul, S. Misra, J. Mandal, M. Dolai and A. Majhi, *Spectrochim. Acta, Part A*, 2025, **336**, 125964.
46 H. Shen, J. Wang, J. Ao, Y. Cai, M. Xi, Y. Hou, M. Li and A. Luo, *LWT*, 2022, **172**, 114179.
47 L. Han, Y. Li, B. Hu, W. Wang, J. Guo, J. Yang, N. Dong, Y. Li and T. Li, *Foods*, 2024, **13**, 1943.
48 S. Paul, N. Sepay, S. Sarkar, P. Roy, S. Dasgupta, P. Saha Sardar and A. Majhi, *New J. Chem.*, 2017, **41**, 15392–15404.
49 A. Rasyid and M. Y. Putra, Yasman, *Kuwait J. Sci.*, 2023, **50**, 615–621.
50 Y. Zhang, Q. Dang, C. Liu, J. Yan, D. Cha, S. Liang, X. Li and B. Fan, *Int. J. Biol. Macromol.*, 2017, **102**, 457–467.
51 T. Piri-Gharaghie, G. Ghajari, M. Hassanpoor, N. Jegargoshe-Shirin, S. Mona, S. Khayati, A. Farhadi-Biregani and A. Mirzaei, *Heliyon*, 2023, **9**, e14149.
52 E. Imperlini, F. Massaro, A. Grifoni, F. Maiurano, A. R. Taddei, S. Borocci, F. Buonocore and F. Porcelli, *Peptides*, 2024, **182**, 171311.
53 Q. Cui, Y. Li, T. Li, J. Yu, G. Shen, X. Sun, M. Zhou and Z. Zhang, *Foods*, 2024, **13**, 2978.
54 S. L. S. X. Shiyan, H. Jinlun and Z. Yongliang, *Food Chem.*, 2021, **362**, 130249.
55 S. A. Sibli, V. P. Panagiotou and C. Makris, *Expert Syst. Appl.*, 2025, **286**, 127853.
56 A. Wisal, N. Saeed, M. Aurongzeb, M. Shafique, S. Sohail, W. Anwar, Z. Basharat, M. Irfan, A. Ullah and S. S. Hassan, *Mol. Genet. Genomics*, 2024, **299**, 34.
57 L. Yang, M. Luo, Z. Liu, Y. Li, Z. Lin, S. Geng and Y. Wang, *Amino Acids*, 2023, **55**, 1317–1331.
58 K. M. Kuo, J. Liu, A. Pavlova and J. C. Gumbart, *J. Phys. Chem. B*, 2023, **127**, 7509–7517.
59 C. L. Curley, T. P. Fedrigoni, E. M. Flaherty, C. J. Woodilla and C. L. Hagan, *Biochem.*, 2021, **60**, 2956–2965.
60 M. E. Walker, W. Zhu, J. H. Peterson, H. Wang, J. Patteson, A. Soriano, H. Zhang, T. Mayhood, Y. Hou, S. Mesbahi-Vasey, M. Gu, J. Frost, J. Lu, J. Johnston, C. Hipolito, S. Lin, R. E. Painter, D. Klein, A. Walji, A. Weinglass, T. M. Kelly, A. Saldanha, J. Schubert, H. D. Bernstein and S. S. Walker, *Nat. Commun.*, 2025, **16**, 3395.
61 Z. Feng, Y. Wang, H. Xu, Y. Guo, W. Xia, C. Zhao, X. Zhao and J. Wu, *Acta Pharm. Sin. B*, 2023, **13**, 1014–1027.
62 A. Garg, R. Tewari and G. P. Raghava, *BMC Bioinf.*, 2010, **11**, 125.
63 J. He, H. Guo, M. Zhang, M. Wang, L. Sun and Y. Zhuang, *Foods*, 2022, **11**, 468.